International Journal of Heat and Fluid Flow 64 (2017) 1–9

Contents lists available at ScienceDirect

International Journal of Heat and Fluid Flow

journal homepage: www.elsevier.com/locate/ijhff

Statistical analysis of the hydrodynamic pressure in the near field of compressible jets

R. Camussi[a], A. Di Marco[a,*], T. Castelain[b]

[a] Università degli Studi Roma TRE, Rome 00146, Italy
[b] École Centrale de Lyon, Lyon 69134 Ecully Cedex, France

ARTICLE INFO

Article history:
Received 26 September 2016
Revised 18 January 2017
Accepted 21 January 2017
Available online 8 February 2017

ABSTRACT

This paper is devoted to the statistical characterization of the pressure fluctuations measured in the near field of a compressible jet at two subsonic Mach numbers, 0.6 and 0.9. The analysis is focused on the hydrodynamic pressure measured at different distances from the jet exit and analyzed at the typical frequency associated to the Kelvin–Helmholtz instability. Statistical properties are retrieved by the application of the wavelet transform to the experimental data and the computation of the wavelet scalogram around that frequency. This procedure highlights traces of events that appear intermittently in time and have variable strength. A wavelet-based event tracking procedure has been applied providing a statistical characterization of the time delay between successive events and of their energy level. On this basis, two stochastic models are proposed and validated against the experimental data in the different flow conditions

1. Introduction

Many studies on jet noise carried out in the last 50 years demonstrated that large-scale vortices formed in the shear layer close to the jet exit contribute to the generation of sound in the radiation to aft angles (see e.g. the seminal papers by Bishop, Ffowcs-Williams and Smith, 1971, and Fuchs, 1972a, Fuchs (1972b Jul 1)). This evidence motivated the search for topologically simple flow structures as sources of jet noise with the scope of setting up reduced-order models able to predict the far-field noise using a limited number of parameters and beneficial for noise control (see e.g. Noack et al., 2011). Although an extensive literature exists on this subject, we still suffer from a lack of knowledge about the precise role of the large-scale structures and the influence of their dynamics in the generation of acoustic waves. Indeed, even though low-order modelling is of relevant interest for practical applications, it becomes challenging for realistic high Reynolds number (*Re*) jets, where the dynamics of the large-scale structures is complex and their statistics non-periodic and non-Gaussian. As outlined by Karney-Fisher et al. (2013) and Karney-Fisher (2015) the non-determinism of the large-scale structures at high *Re* increases the number of parameters that influences jet noise and thus prevents the possibility to build up reliable low-order theoretical models. The complex dynamics at high *Re* is mainly related to the intermittent appearance of the flow structures (e.g. Karney-Fisher, 2015) and the space-time jitter affecting their topological properties (e.g. Cavalieri et al., 2011b). It must be pointed out that the intermittent nature of the noise sources is a well-known property that has been recognized since many years as a fundamental ingredient to be taken into account far accurate jet noise modeling (see e.g. the seminal paper by Juve et al., 1980).

From the topological viewpoint, many researchers have recognized that flow structures associated with the jet mixing noise are localized wave-packets convected downstream at a quasi-constant velocity and originated by the jet column axisymmetric mode (see the recent review by Jordan and Colonius 2013, and the reference therein for the details). Wave-packets are known to be related to the jet Kelvin–Helmholtz instability, and exhibit growth, saturation and decay with specific topological parameters (see Reba et al., 2010). However, as shown in several recent papers (Hileman et al., 2005; Kastner et al., 2006; Suponitsky, Sandham & Morfey 2010; Cavalieri et al., 2011a), intermittency at high *Re* affects the dynamics of the wave-packets and governs the statistics of their physical properties. Due to the multiscale and strongly unsteady nature of turbulence, a clear picture of the wave-packets statistics at high *Re* is still far to be reached and the main objective of the present work is to shed light on this aspect.

Insights into the wave-packet dynamics at high *Re* can be retrieved by analyzing the near-field hydrodynamic pressure measured or computed nearby the jet exit. Indeed, as shown in the seminal experiment by Laufer and Yen (1983) on a forced jet, the near-field pressure has a wave-packet shape resulting as a

* Corresponding author.

http://dx.doi.org/10.1016/j.ijheatfluidflow.2017.01.007
0142-727X/

combination of oscillations at the frequency of the principal instability modes and a Gaussian envelope. The near field pressure has been used by Chrighton and Huerre (1990) to examine the far-field acoustic super-directivity of wave-packets, a concept recently recovered by Cavalieri et al. (2012). In the Fourier domain, the low frequency region of the near-field pressure spectra is dominated by the hydrodynamic pressure component whereas high frequencies are associated to acoustic pressure waves (see e.g. Arndt et al., 1997, Grizzi and Camussi, 2012). The hydrodynamic part of the spectrum is directly influenced by the wave-packets and typically exhibits a bump around the Kelvin–Helmholtz frequency, that corresponds to a Strouhal number around 0.3 (see e.g. Cavalieri et al., 2013). Intermittency is reflected into the non-peaked Fourier spectrum of the hydrodynamic pressure around the Kelvin–Helmholtz frequency.

As outlined above, the hydrodynamic events that radiate noise at aft angles are intermittent bursts appearing randomly in time and space as opposed to regions of relatively quiet background (Karney-Fisher, 2015). Due to their localized nature, the use of wavelet transform rather than Fourier analysis is straightforward for their identification. The success of the wavelet analysis for the extraction of pressure events has been demonstrated in several previous works (e.g. Koenig et al., 2013, Grizzi and Camussi, 2012, Lewalle et al., 2012, Mancinelli et al., 2016). Of specific interest for the present paper is the work by Cavalieri et al. (2011a) who analyzed the wavelet transform of the azimuthal zero-order mode of the acoustic pressure and the recent paper by Kearney-Fisher (2015) who applied the wavelet transform to the far field pressure to retrieve the statistics of the intermittent events. Their results confirmed the capability of the wavelet decomposition to isolate localized events important for the production of sound. The present paper extends their approach to the near field pressure. To this aim, near field pressure data measured close to a compressible single stream jet at subsonic Mach numbers, are analyzed using the wavelet transform. The present approach focalizes onto the statistics of low frequency intermittent events that are known to be associated to hydrodynamic pressure fluctuations (Arndt et al., 1997). Therefore, a separation between hydrodynamic and acoustic pressure is not required for their characterization. The square of the wavelet coefficients is extracted around the Kelvin–Helmholtz frequency and used to retrieve statistical properties and stochastic models of relevant features of the flow structures.

A more detailed description of the procedure adopted for the data analysis is given in the next section. Results are presented in Section 3 where a parametric study in terms of Mach number and distance from the jet exit is presented. The main conclusions are given in Section 4.

2. Experimental data-base and post-processing procedure

The database analyzed have been obtained in an experimental campaign carried out at the anechoic wind tunnel of the Laboratoire de Mecanique des Fluides et d' Acoustique of the Ecole Centrale de Lyon. The data refer to measurements of the near-field pressure of a single-stream round jet having diameter $D = 50$ mm. The near-field pressure was measured at two Mach numbers, 0.6 and 0.9, using a linear array of 14 microphones placed at a radial distance $1.2D$ from the jet axis measured at the nozzle exit. The array was aligned to the jet spreading angle, inclined of 11° with respect to the jet axis and the microphones position spanned an axial distance from $x/D = 2$ to $x/D = 8.7$, $x = 0$ being the nozzle exhaust. Pressure data were acquired at a sampling frequency equal to 51.2 kHz and for an acquisition time of 10 s. More details about the experimental set up can be found in Mancinelli et al. (2016) where a comprehensive aerodynamic and aeroacoustic jet flow qualification is also presented.

In addition to standard data processing procedures based on the Fourier decomposition, the present approach includes the use of the wavelet transform that has been applied to the pressure data to retrieve the energy scalogram, a 2D representation of the energy contained by the signal. More specifically, the wavelet decomposition of a signal $p(t)$ at the resolution time scale s is given by the following expression.

$$w(s,t) = \frac{1}{\sqrt{s}} \int_{-\infty}^{+\infty} \Psi^*\left(\frac{\tau - t}{s}\right) p(t) d\tau$$

where the integral represents a convolution between $p(t)$ and the dilated and translated complex conjugate counterpart of $\Psi(t)$. The wavelet scalogram is given by the square of the wavelet coefficients and it provides a decomposition of the energy onto the (s,t) plane. As reported in Farge (1992), the scalogram provides a localized counterpart of the standard Fourier spectrum that can be recovered by a simple time integration. A sketch of this concept is given in Fig. 1 where it is clarified that the analysis of the scalogram at a fixed s provides the evolution in time of the Fourier mode corresponding to the frequency $1/s$.

An example of the Fourier spectrum recovered from the wavelet scalogram plotted against the standard Power spectrum is reported in Fig. 2 showing a very good agreement.

Several wavelet types have been tested and the continuous transform using a Morlet kernel has been selected since it provides the best accuracy in reproducing the Fourier spectrum. It has been checked that the results do not depend on the choice of the wavelet kernel neither on the continuous or discrete nature of the wavelet type adopted.

The wavelet scalogram is the key quantity analyzed in the present work since its amplitude, at a given s, is used to select events through a simple search-of-maxima algorithm. More details on this procedure are given in the following section.

3. Results

As reported in Arndt et al., (1997) in the near field region of the jet, the low frequency region of the spectra is associated to the hydrodynamic pressure and it is dominated by the energy contained around the frequency associated to the Kelvin–Helmholtz instability, hereafter denoted as f_{kh}. The example reported in Fig. 2, corresponding to a pressure signal acquired at $x/D = 2$ and $M_j = 0.6$, indeed exhibits a bump around 1500 Hz corresponding to $St \approx 0.2$, where St denotes the Strouhal number computed using the jet diameter D and the jet exit velocity.

Scalograms corresponding to a segment of the signal measured at $x/D = 2$ for the two Mach numbers analyzed therein are reported in Fig. 3. It is evident that also the wavelet decomposition highlights that most of the energy is contained at the frequency f_{kh}. The most interesting feature is that the temporal evolution of the energy at that frequency is strongly intermittent since bursts of high energy are alternated to relatively low energy intervals.

This behavior is further highlighted through a band-pass digital filtering around f_{kh}. The analysis of the filtered signals permits to verify that the energy bumps evidenced in the wavelet scalogram correspond to variations of the amplitude modulation of wave-packets. This is shown in Fig. 4 where a segment of a filtered pressure signal is reported as well as the corresponding scalogram. This plot demonstrates the capability of the scalogram to enhance localized amplitude fluctuations modulating the oscillations at the frequency f_{kh}. Similar results are obtained in the other microphone positions and Mach number and are not reported in the following for the sake of brevity.

This property is used to extract the temporal location of the events. The burst tracking is indeed performed by a simple search of maxima of the scalogram at the frequency f_{kh}, each relative

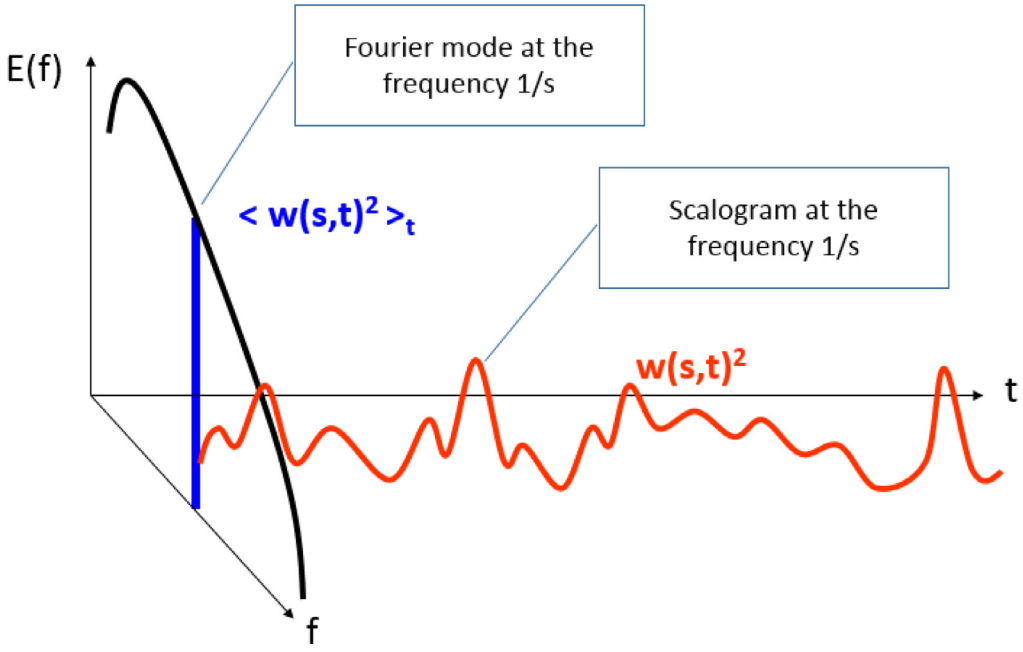

Fig. 1. A sketch clarifying the physical meaning of the wavelet scalogram. The symbol $<..>_t$ denotes a time average. The mean value of the squared wavelet coefficients corresponds to the amplitude of the Fourier modes.

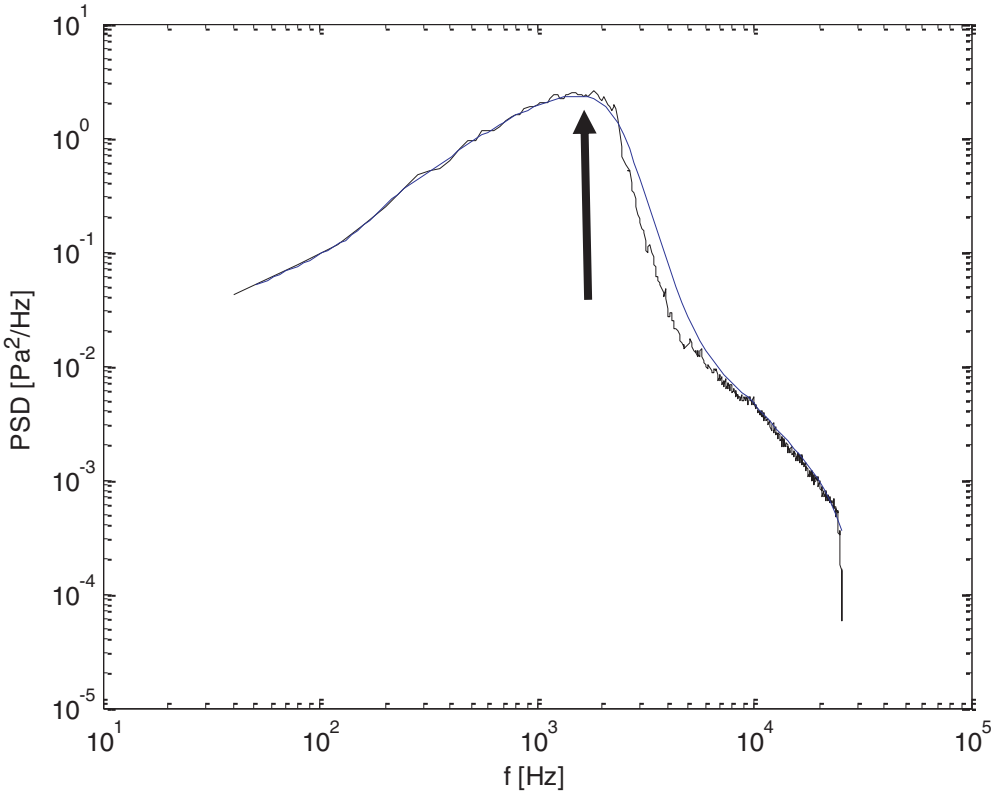

Fig. 2. Example of wavelet spectrum (blue line) compared with a standard Fourier spectrum (black line). The wavelet transform has been obtained using the Morlet kernel and the measurement parameters are $x/D=2$ and $M_j=0.6$. The arrow points toward the frequency f_{kh} where the spectra reach the maximum. (For interpretation of the references to colour in this figure legend, the reader is referred to the web version of this article.)

maximum providing the temporal location of the event and of its energy content. It must be pointed out that events are collected on the basis of their energy content in the wavelet domain, with no a-priori assumptions on their physical nature. The relationship between the selected events and flow structures of specific topology is based on the consolidated idea that most of the energy contained at the Kelvin–Helmholtz frequency is associated to wave-packets appearing intermittently in time and space (see e.g. Jordan and Colonius 2013).

The time of appearance is sequentially collected in a set from which the time delay Δt between two successive events can be easily computed. Kearney-Fischer et al., (2013) denoted this pa-

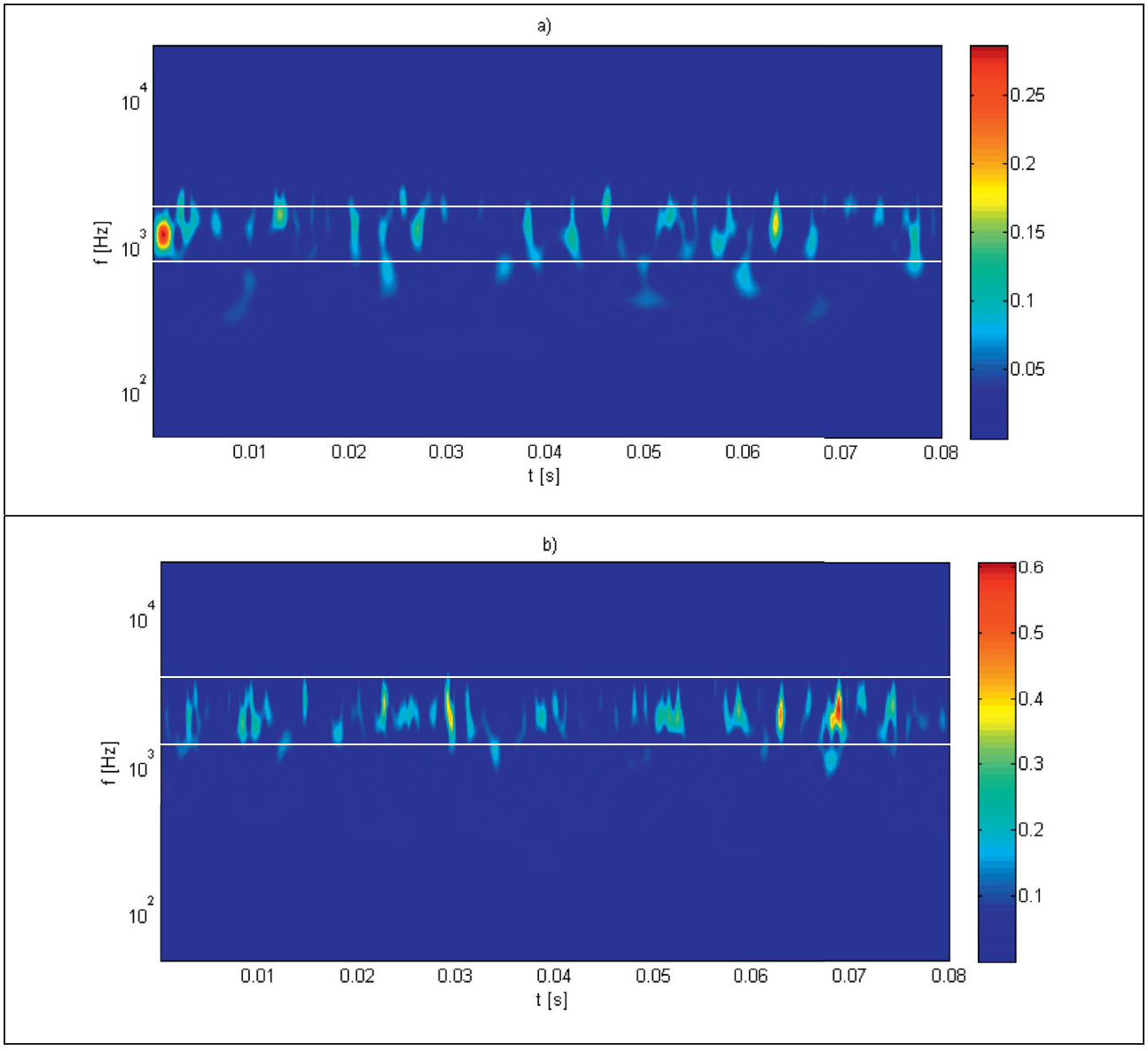

Fig. 3. Example of a scalogram computed from a segment of a signal measured at $x/D=2$ for $M_j=0.6$ (a) and $M_j=0.9$ (b). The white lines enclose the frequency range of the bump centered on f_{kh}. (For interpretation of the references to colour in this figure legend, the reader is referred to the web version of this article.)

rameter as intermittence, since its statistics provides a direct estimation of the intermittent degree of the phenomenon causing the selected events. The normalized Probability Distribution Functions (PDF) of this random variable are reported in Figs. 5 and 6 for $M_j=0.6$ and 0.9 respectively and for different distances from the jet exit. The PDFs are plotted in normalized variables, that is by subtracting the mean value of the signal and dividing by its standard deviation.

It is shown that the shape of the PDFs does not change significantly either for different distances from the jet or for the different Mach numbers. Among various possibilities, it has been checked that the best approximation of the PDFs, except for small Δt, can be achieved by using a log-normal representation and a reference curve is reported in Figs. 5 and 6 for comparison. It should be stressed that Kearney-Fischer et al., (2013) adopted a gamma function to approximate the Δt distribution but in their case the events where extracted in the far field.

A log-normal distribution is characterized by two parameters, m and v (see Feller, 1950), representing the so-called PDF location and shape respectively. For each test case presently analyzed, the two parameters have been computed through a maximum likelihood estimation and the results achieved at $M_j=0.6$ and $M_j=0.9$ are reported in Fig. 7, as functions of the distance from the jet. For the $M_j=0.6$ case, distances overcoming $x/D=6$ are not reported because data appeared not to have statistically converged. The reason is because at low velocity and large distances from the nozzle exit the number of selected events tend to diminish. The mean value $\langle\Delta t\rangle$ and the standard deviation of Δt, denoted as $\sigma_{\Delta t}$, are presented as well in the same figures. It is observed that the amplitude of the parameters, including the mean value $\langle\Delta t\rangle$, increases monotonically and almost linearly with x/D, even though the slope of curves is very small. This means that the variation of the parameters is not relevant but, whenever required, it can be approximated through a simple analytical linear function. It is also noticed that the lower the Mach number the larger the amplitude of all the parameters, even though, also from the view point of the Mach number effects, the variations are small.

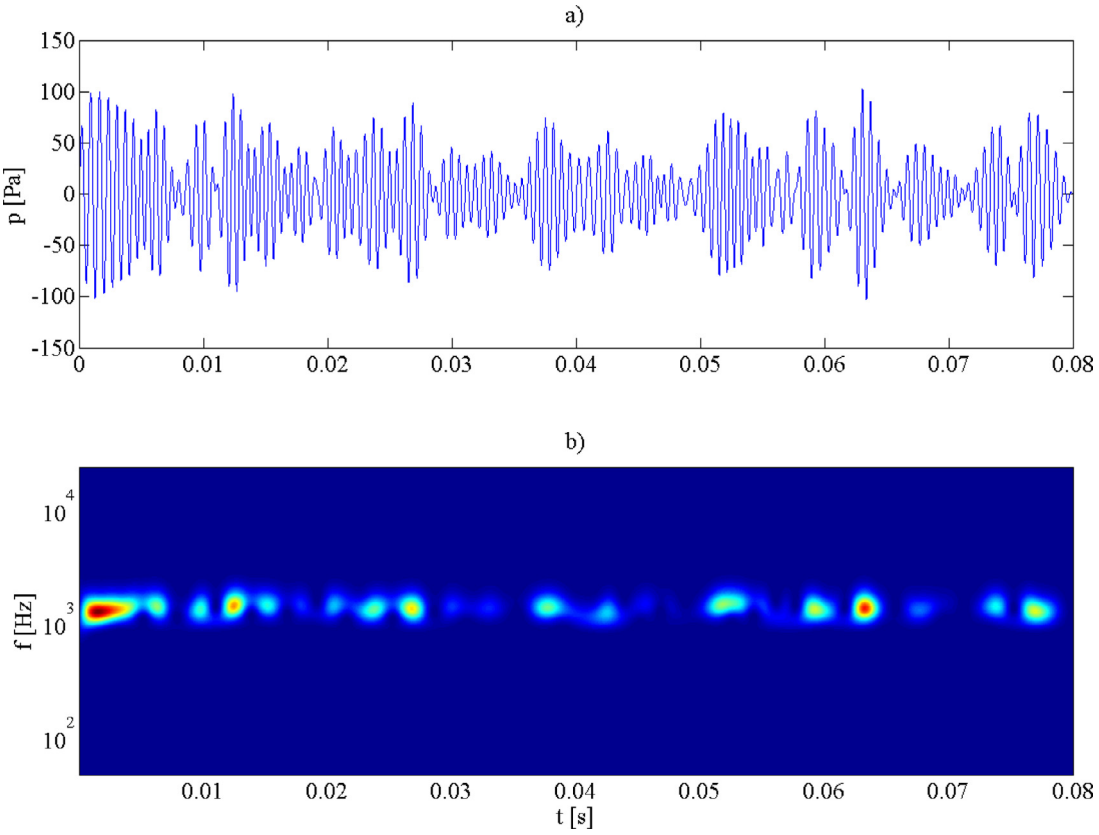

Fig. 4. Example of a segment of a signal at $x/D=2$ for $M_j=0.6$ and filtered around f_{kh} (a) and its corresponding scalogram (b).

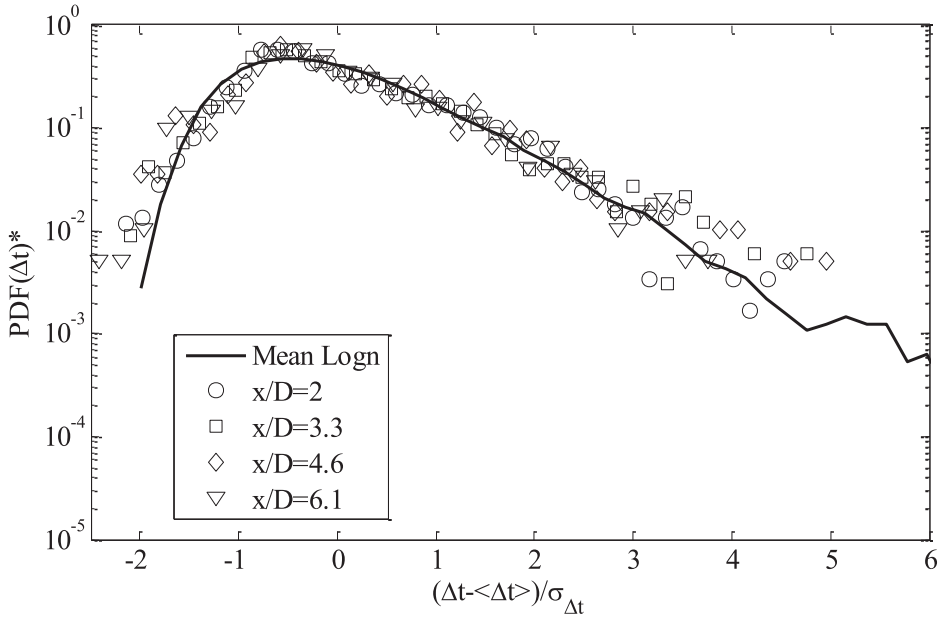

Fig. 5. PDF of the time delay between events for different distances at $M_j=0.6$. The solid black line represents a reference log-normal distribution based on the averaged values of the log-normal parameters reported in Table 1. (For interpretation of the references to color in this figure legend, the reader is referred to the web version of this article.)

The mean value of the parameters, averaged over the whole set of test cases analyzed, together with the corresponding standard deviations, are reported in Table 1. The values of the parameters are averaged over the whole distances x/D and were used to plot the reference PDFs in Figs. 5 and 6.

The numerical values reported in Table 1 confirm that the amplitude of the parameters does not change significantly for the different flow conditions. Therefore, a log-normal PDF with the parameters reported in Table 1, represents a reliable stochastic model of the variable Δt and can be used to predict with a reasonable accuracy its statistical properties.

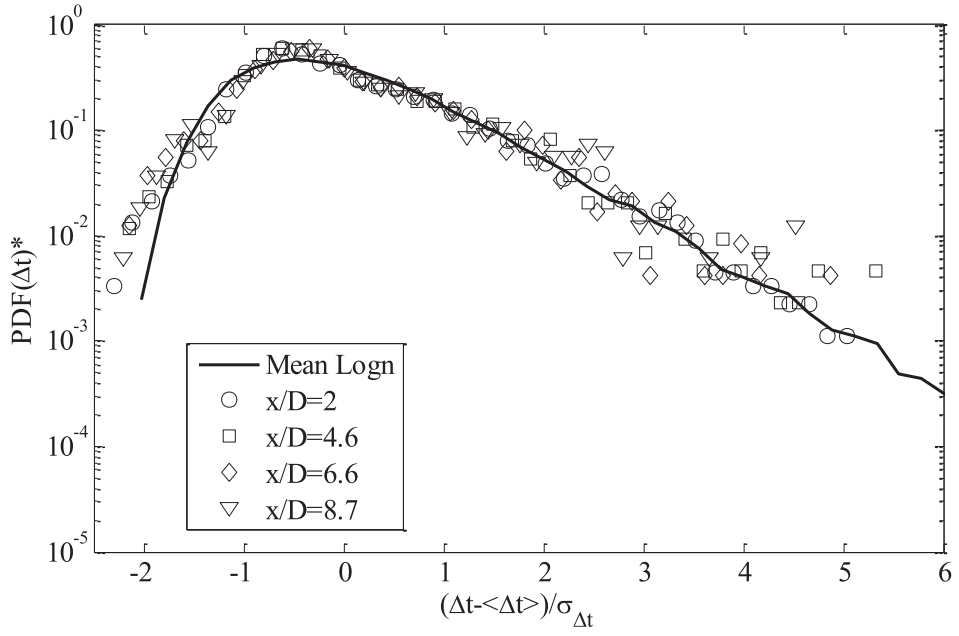

Fig. 6. Same as previous plot but for $M_j = 0.9$.

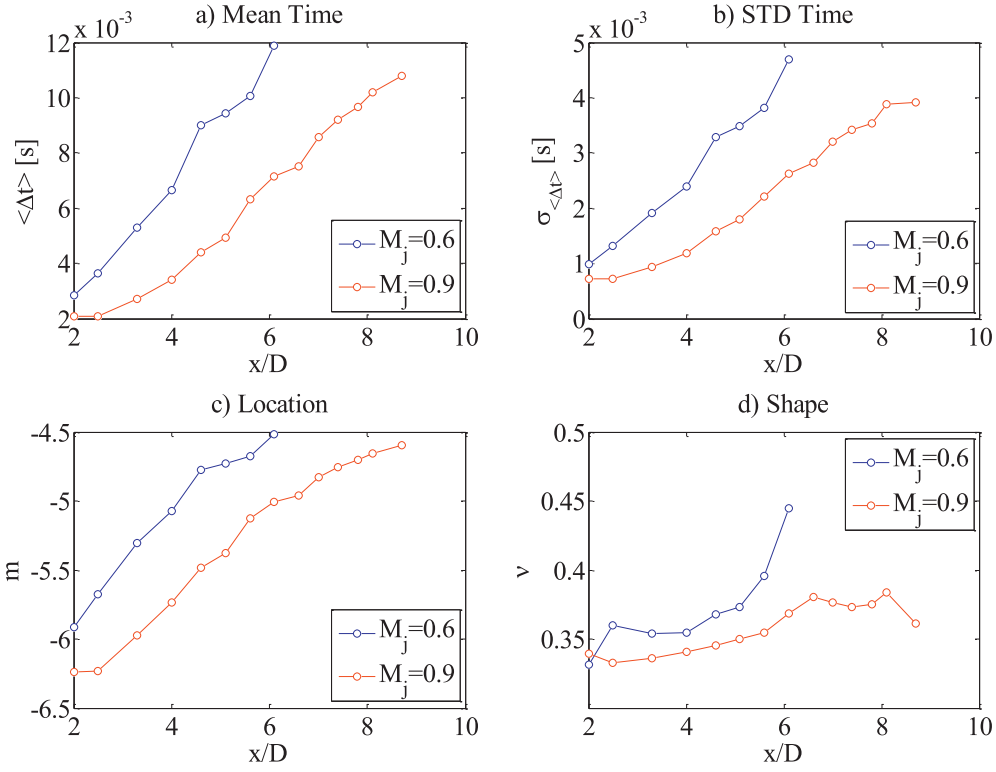

Fig. 7. Comparison of the log-normal PDF parameters at $M_j = 0.6$ and $M_j = 0.9$ for the microphone positions considered. (For interpretation of the references to color in this figure legend, the reader is referred to the web version of this article.)

Table 1
Parameters characterizing the log-normal PDF of the intermittence variable Δt.

Mach number	Parameters		Uncertainty (standard deviation))
$M_j = 0.6$	$<\Delta t>$	0.0059	0.0038
	m	−5.0831	0.5084
	v	0.3727	0.0343
$M_j = 0.9$	$<\Delta t>$	0.0047	0.0034
	m	−5.2624	0.5836
	v	0.3585	0.0178

It can be noted that the uncertainty associated to Δt is relatively very large. However, it should be stressed that the relatively large amplitude of the standard deviation is not related to a lack of statistical convergence but rather to the shape of the PDF that is strongly skewed and has a very pronounced tail towards positive values. This renders in this case the standard deviation a non-meaningful estimator of the data uncertainty.

An analogous approach has been adopted for the stochastic modelling of the amplitude of the events, denoted as A. As outlined above, the amplitude is retrieved from a simple search of maxima

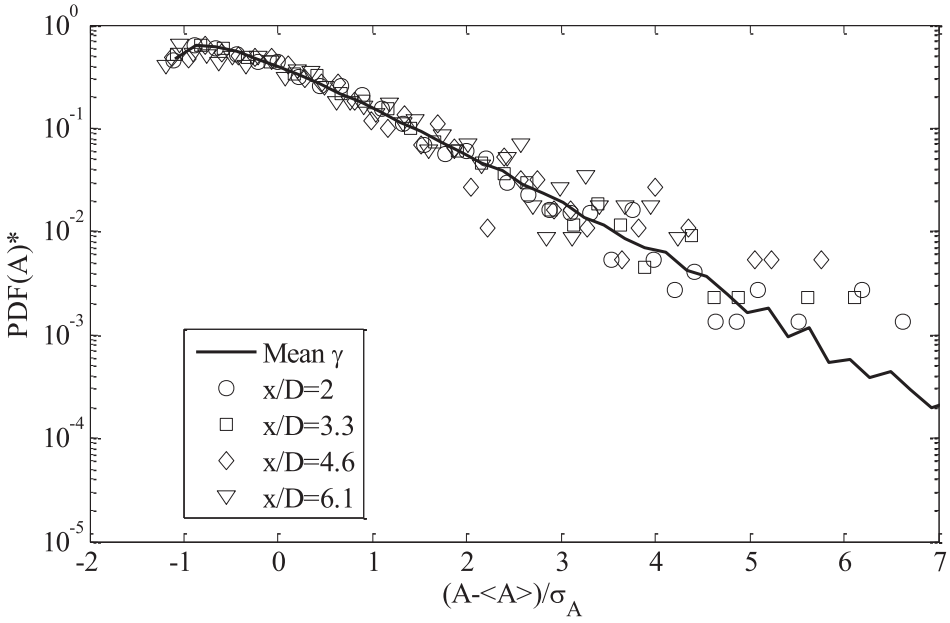

Fig. 8. PDF of the events amplitude for different distances at $M_j = 0.6$. The solid black line represents a reference gamma distribution based on the averaged values of the gamma parameters reported in Table 2. (For interpretation of the references to color in this figure legend, the reader is referred to the web version of this article.)

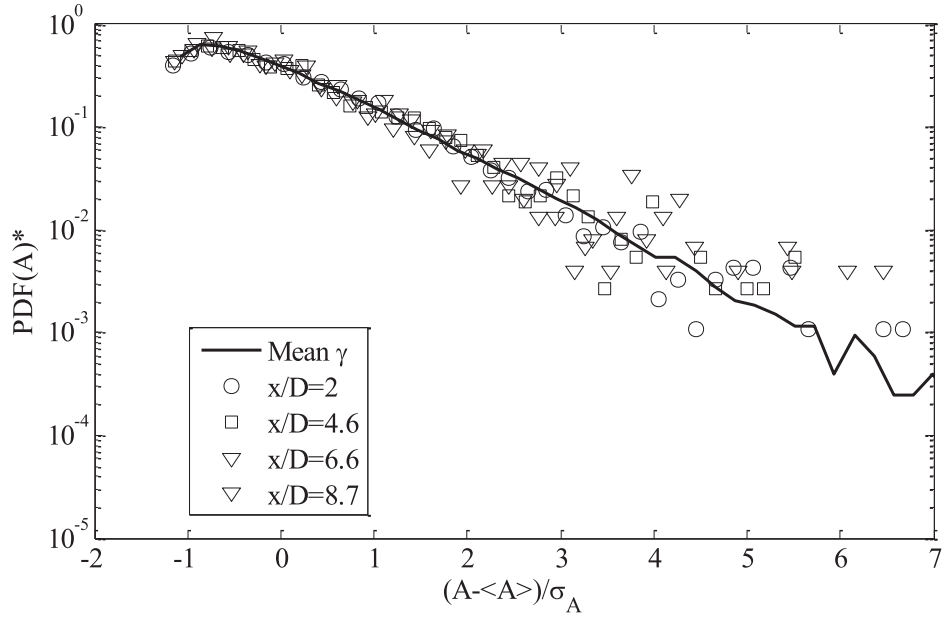

Fig. 9. Same as previous plot but for $M_j = 0.9$.

of the scalogram at f_{kh}, each maximum providing the energy content of the selected events. As pointed out above, this quantity has a very important physical meaning since it represents the instantaneous value of the most energetic Fourier mode, i.e. the one corresponding to the frequency associated to the Kelvin–Helmholtz instability. PDFs of the variable A are reported in Figs. 8 and 9 for $M_j = 0.6$ and 0.9 respectively.

In the case of the random variable A, the reference analytical approximation is given by a Gamma distribution, again characterized by two quantities, l and ξ, that are named the shape and the scale respectively (see Feller, 1950, and Kearney-Fischer et al., 2013). The parameters as functions of the distance from the jet exit are reported in Fig. 10 for $M_j = 0.6$ and 0.9 and their averaged values are summarized in Table 2. Fig. 10 shows that, except for the shape l, the parameters increase almost linearly with x/D but, contrary to the previous case, they are larger for larger M. This behavior can be ascribed to the higher energy contained by the flow structures at higher velocities. At the higher M, the energy variations increase and also induce larger fluctuations (see Fig. 10b).

Table 2
Parameters characterizing the gamma PDF of the amplitude A.

Mach number	Parameters		Uncertainty (standard deviation))
$M_j = 0.6$	$<A>$	0.0595	0.0523
	l	1.4324	0.0632
	ξ	0.0464	0.0099
$M_j = 0.9$	$<A>$	0.1559	0.1354
	l	1.4253	0.0723
	ξ	0.1242	0.0283

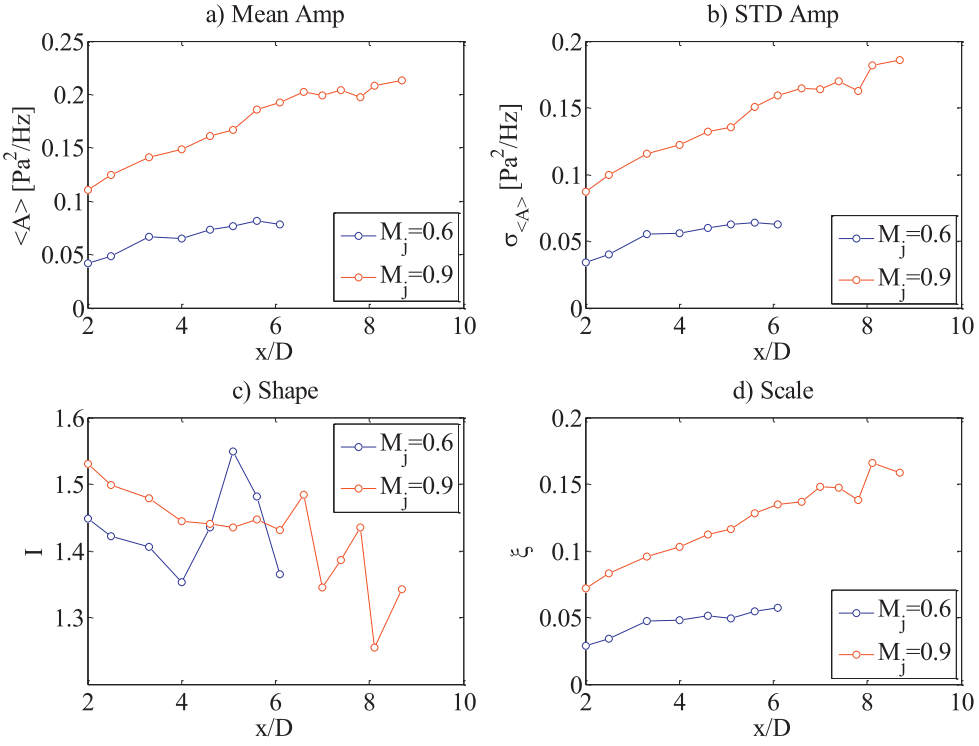

Fig. 10. Comparison of the gamma PDF parameters at $M_j = 0.6$ and $M_j = 0.9$ for the microphone positions considered. (For interpretation of the references to color in this figure legend, the reader is referred to the web version of this article.)

As for the previous case, it is observed that the amplitude variation of the parameters with x/D is relatively small. Therefore, the averaged parameters reported in Table 2 can be used for setting up a reliable stochastic model of the events amplitude A for each Mach number. As for the previous case, the model takes into account only the increase of the scale parameter with the Mach number but not their dependence upon x/D. The mean values of the parameters of Table 2 are used to plot the reference PDFs in Figs. 7 and 8 and the reliability of these results confirm the validity of this approach.

Figs. 7 and 10 suggest that it is possible to improve the stochastic modeling of Δt and A by taking into account the dependence of the parameters of the PDFs upon the position and the flow velocity. However, this generalization would increase considerably the degree of complexity of the models without improving significantly their predictive ability. Nonetheless, if a higher degree of accuracy is required, the dependence upon x/D can be determined whereas the functional dependence of the PDFs parameters upon M cannot be driven from the present data set. To this purpose, further data taken at different flow conditions are surely needed.

4. Conclusions

In the present study the near field pressure fluctuations measured in the vicinity of a single stream jet at $M_j = 0.6$ and 0.9 are analyzed using Fourier transform and wavelet decompositions. The study is targeted to characterize the Fourier mode at the frequency where the energy is maximum that is the frequency associated to the Kelvin–Helmholtz instability process. The temporal evolution of the energy is achieved by the computation of the wavelet scalogram, providing a 2D representation of the energy contained by the signal and computed by the time-frequency distribution of the squared wavelet coefficients. It is observed that the near-field pressure around the Fourier energy bump is characterized by localized intermittent events that are traces of wave-packets appearing randomly in time. The statistics of these structures have been characterized by selecting energetic events from the wavelet scalogram at the frequency of maximum energy. The selected events are used to retrieve two important random variables, the time interval between two successive events, Δt, and the amplitude of their energy content, A. The statistics of these random variables provide statistical properties that are useful to build up stochastic models able to reproduce and predict the wave-packet dynamics.

The analysis of Δt shows that the PDF does not depend significantly on the distance from the jet and upon the Mach number. The best fit of the normalized PDF is provided by a log-normal distribution whose parameters, the so-called location and shape, are determined by a maximum likelihood estimation and an average over the different flow conditions. The parameter A is analyzed in a very similar manner. Also in this case the shape of the PDF is weakly dependent upon the position and the Mach number but the best approximation is achieved by a Gamma distribution. The maximum likelihood estimation and the average over the whole set of flow conditions provides the parameters of the distribution, i.e. the shape and the scale.

The analysis of the PDFs parameters have shown that a more accurate and general modeling can be achieved by taking into account the effects of the distance x/D and of the Mach number. Specifically, for both variables, Δt and A, a close to linear dependence of the parameters upon the distance from the jet exit is observed. On the other hand, due to the limited number of cases studied, a clear definition of the dependence upon the Mach number has not been achieved and this remains a task for future studies.

Acknowledgments

The authors acknowledge the support of the EU Collaborative project ORINOCO (ACP0-GA-2010-266103) and the partial support of the EU Collaborative project JERONIMO (ACP2-GA-2012-314692).

Both the projects have been funded under the EU 7th Framework Program.

Olivier Leon is acknowledged for his work during the experimental test campaign.

References

Arndt, REA., Long, D.F., Glauser, M.N., 1997 Jun. The proper orthogonal decomposition of pressure fluctuations surrounding a turbulent jet. J. Fluid Mech. 340, 1–33.

Bishop, K.A., Williams, J.E.F., Smith, W., 1971 Nov. On the noise sources of the unsuppressed high-speed jet. J. Fluid Mech. 50 (1), 21–31.

Cavalieri, A.V.G., Daviller, G., Comte, P., Jordan, P., Tadmor, G., Gervais, Y., 2011a Aug 15. Using large eddy simulation to explore sound-source mechanisms in jets. J. Sound Vibr. 330 (17), 4098–4113.

Cavalieri, A.V.G., Jordan, P., Agarwal, A., Gervais, Y., 2011b Sep 12. Jittering wave–packet models for subsonic jet noise. J. Sound Vibr. 330 (18-19), 4474–4492.

Cavalieri, A.V.G., Jordan, P., Colonius, T., Gervais, Y., 2012. Axisymmetric superdirectivity in subsonic jets. J. Fluid Mech. 704, 388–420.

Cavalieri, A.V.G., Rodríguez, D., Jordan, P., Colonius, T., Gervais, Y., 2013 Sep. Wave packets in the velocity field of turbulent jets. J. Fluid Mech. 730, 559–592.

Crighton, D.G., Huerre, P., 1990 Nov. Shear-layer pressure fluctuations and superdirective acoustic sources. J. Fluid Mech. 220, 355–368.

Farge, M., 1992. Wavelet Transforms and their applications to turbulence. Annu. Rev. Fluid Mech. 24 (1), 395–458.

Feller, W., 1950. An Introduction to Probability Theory and Its Applications, Volume 1, 3rd Edition Wiley.

Fuchs, H.V., 1972a Jun 1. Measurement of pressure fluctuations within subsonic turbulent jets. J. Sound Vibr. 22, 361–378.

Fuchs, H.V., 1972b Jul 1. Space correlations of the fluctuating pressure in subsonic turbulent jets. J.Sound Vibr. 23, 77–99.

Grizzi, S., Camussi, R., 2012 May. Wavelet analysis of near-field pressure fluctuations generated by a subsonic jet. J. Fluid Mech. 698, 93–124.

Hileman, J.I., Thurow, B.S., Caraballo, E.J., Samimy, M., 2005 Dec. Large-scale structure evolution and sound emission in high-speed jets: real-time visualization with simultaneous acoustic measurements. J. Fluid Mech. 544, 277–307.

Jordan, P., Colonius, T., 2013. Wave packets and turbulent jet noise. Annu. Rev. Fluid Mech. 45 (1), 173–195.

Juvé, D., Sunyach, M., Comte-Bellot, G., 1980 Aug 8. Intermittency of the noise emission in subsonic cold jets. J. Sound Vibr. 71 (3), 319–332.

Kastner, J., Samimy, M., Hileman, J., Freund, J.B., 2006. Comparison of noise mechanisms in high and low Reynolds number high-speed jets. AIAA J. 44 (10), 2251–2258.

Kearney-Fischer, M., Sinha, A., Samimy, M., 2013. Intermittent nature of subsonic jet noise. AIAA J. 51 (5), 1142–1155.

Kearney-Fischer, M., 2015 Mar 3. A model function for jet noise events at aft angles and what it says about the statistical relationships of the events. J. Sound Vibr. 338, 217–236.

Kœnig, M., Cavalieri, A.V.G., Jordan, P., Delville, J., Gervais, Y., Papamoschou, D., 2013 Sep 2. Farfield filtering and source imaging of subsonic jet noise. J. Sound Vibr. 332 (18), 4067–4088.

Laufer, J., Yen, T-C., 1983 Sep. Noise generation by a low-Mach-number jet. J. Fluid Mech 134, 1–31.

Lewalle, J., Low, K.R., Glauser, M.N., 2012 Oct 1. Properties of the far-field pressure signatures of individual jet noise sources. Int. J. Aeroacoust 11 (5-6), 651–674.

Mancinelli, M., Pagliaroli, T., Di Marco, A., Camussi, R., Castelain, T., Leon, O., 2016. Hydrodynamic and acoustic wavelet-based separation of the near-field pressure of a compressible jet. 22nd AIAA/CEAS Aeroacoustics Conference. American Institute of Aeronautics and Astronautics, pp. 1–18. AIAA 2016-2864.

Noack, B., Morzynski, M., Tadmor, G., 2011. Reduced-Order Modelling for Flow Control. CISM Courses Lect, 528. Springer-Verlag, Berlin.

Reba, R., Narayanan, S., Colonius, T., 2010 Jun 1. Wave-packet models for large-scale mixing noise. Int. J. Aeroacoust. 9 (4-5), 533–557.

Suponitsky, V., Sandham, N.D., Morfey, C.L., 2010 Sep. Linear and nonlinear mechanisms of sound radiation by instability waves in subsonic jets. J. Fluid Mech. 658, 509–538.